Measuring 3-dimensional dynamics of membrane in living cell with metal-induced energy transfer imaging/spectroscopy

Tao Chen[1*], José Ignacio Gallea[1], Narain Karedla[2,3], Dongxia Wang[1,4] and Jörg Enderlein[1,5*]

[1]Third Institute of Physics – Biophysics, Georg August University, Friedrich-Hund-Platz 1, Göttingen, 37077, Germany.
[2]The Rosalind Franklin Institute, Harwell Campus, Didcot, OX11 OFA, UK.
[3]Kennedy Institute of Rheumatology, University of Oxford, Roosevelt Drive Oxford, OX3 7LF, UK.
[4]Tianjin Key Laboratory of Biosensing and Molecular Recognition, Frontiers Science Center for Cell Responses, Research Centre for Analytical Sciences, College of Chemistry, Nankai University, 94 Weijin Rd, Nankai District Tianjin, 300071, P. R. China.
[5]Cluster of Excellence "Multiscale Bioimaging: from Molecular Machines to Networks of Excitable Cells" (MBExC), Universitätsmedizin Göttingen, Robert-Koch-Str. 40, Göttingen, 37075, Germany.

*Corresponding author(s). E-mail(s): tao.chen@phys.uni-goettingen.de; jenderl@gwdg.de;

Abstract

The dynamics of cellular membranes are crucial for many essential cellular processes. Despite various methods available to study membrane dynamics, simultaneously measuring membrane diffusion and fluctuations within living cell membranes remains challenging. In this study, we developed a method combining metal-induced energy transfer (MIET) with fluorescence correlation spectroscopy (FCS) to accurately measure the three-dimensional (3D) dynamics of membranes, including

transverse diffusion and vertical fluctuations. Our approach achieves a spatiotemporal resolution of one nanometer and few microseconds. We demonstrate the efficacy of our technique through experiments on the diffusion and transversal undulations of model membranes. Additionally, we showcase the versatility of MIET-FCS by applying it to various membrane systems within living cells, such as the plasma membrane, endoplasmic reticulum, and nuclear envelope. Our findings provide a powerful tool for investigating complex membrane dynamics in diverse cellular environments, advancing the field of membrane biophysics.

Keywords: membrane biophysics, fluorescence correlation spectroscopy, super-resolution microscopy, fluorescence lifetime microscopy, membrane dynamics

Introduction

Biological membranes are dynamic entities, not static structures. They are composed of lipids and numerous membrane proteins that form a very dynamical system. The motions of membrane constituents are essential for critical cellular functions such as cell adhesion, maintaining fluidity and flexibility, responding to external stimuli, molecular transport, and trafficking. Significantly, abnormalities in membrane dynamics are linked to various diseases [1–3]. Cancer cell membranes, for example, are more prone to bending, stretching, and perforation than those of healthy cells [4].

The dynamics of membranes encompasses a large range of length and time scales, from molecular rotations of proteins and lipids [5, 6], or lipid flip-flops between leaflets [7, 8], to membrane-level lateral diffusion [9, 10], vertical fluctuations, and bending [11, 12]. At the cellular level, membrane dynamics are intricately associated with dynamic interactions with the cytoskeleton [13]. Understanding membrane dynamics provides insights into cellular health, including mechanical properties, disease states associated with membranes, drug responses, cytoskeletal interactions, molecular transport processes, and fundamental biological phenomena [14–19].

Current techniques of studying membrane dynamics are limited as they usually target specific aspects of membrane dynamics. For example, fluorescence recovery after photobleaching (FRAP) [20], fluorescence correlation spectroscopy (FCS) [21], and fluorescence single-molecule tracking (SMT) [22] are designed to measure molecular diffusion in membranes. Conversely, other methods such as fluorescence interference contrast microscopy (FLIC) [23–25], contour analysis [26], flicker spectroscopy [27], diffraction phase microscopy (DPM) [28, 29], reflection interference contrast microscopy (RICM) [30–32], time-resolved membrane fluctuation spectroscopy (TRMFS) [33, 34], and dynamic optical displacement spectroscopy (DODS) [11] focus on measuring

membrane fluctuations [11]. A method that enables the simultaneous measurement of both molecular diffusion and membrane fluctuations, however, is lacking.

This study introduces an innovative approach to concurrently quantify nanoscale molecular diffusion *and* membrane fluctuations with sub-millisecond temporal resolution. The method integrates metal-induced energy transfer imaging/spectroscopy (MIET) [35] with fluorescence correlation spectroscopy (FCS). In a prior study, we demonstrated the effectiveness of MIET and graphene-induced energy transfer (GIET) for quantifying membrane fluctuations using high-concentration dye labeling [36]. However, achieving high-concentration dye-labeling, especially in living cells, is challenging and potentially phototoxic. Furthermore, the labeling with high dye-concentration prevents diffusion measurements with FCS. The MIET-FCS method proposed here overcomes these challenges, allowing measurements at any dye concentration, including low concentrations of fluorescence proteins as suitable for live cell studies.

MIET operates on the electrodynamic coupling of a fluorescent emitter to surface plasmons in a thin metal film (Figure 1a). This coupling results in a pronounced modulation of the excited state lifetime and brightness of the fluorophore, depending on its distance from the metal layer (see Figure 1b). When performing a FCS measurement on a fluorescently labeled membrane in proximity to the metal layer, the transverse diffusion of labeled lipids as well as the vertical fluctuations of the entire membrane will be discernible as characteristic partial decays in the fluorescence intensity autocorrelation.

To demonstrate the efficacy of the method, we measured membrane fluctuations of model giant unilamellar vesicles (GUVs). We compared the observed lipid diffusion and membrane fluctuations with results obtained from various established methods. Subsequently, we applied MIET-FCS to three different membrane systems, both in living and fixed cells: (i) the basal plasma membrane (PM), (ii) the endoplasmic reticulum (ER), and (iii) the nuclear envelope (NE).

Result

Principle of MIET-FCS for measuring the 3D dynamics of membranes

Figure 1 illustrates the MIET setup. The MIET substrate is a conventional microscope coverslip covered with a thin metal film. Fluorescence excitation and detection are done through the metal film from below (epi-fluorescence setup) utilizing a high numerical aperture objective. For excitation, a pulsed white-light laser with ca. 50 ps pulse width and 20 MHz repetition rate equipped with an acousto-optical filter for wavelength selection is used. Collected fluorescence is focused through a pinhole for confocal detection and then recorded with a single-photon avalanche diode (SPAD) in single-photon counting mode. The time delay between laser excitation pulses and detected

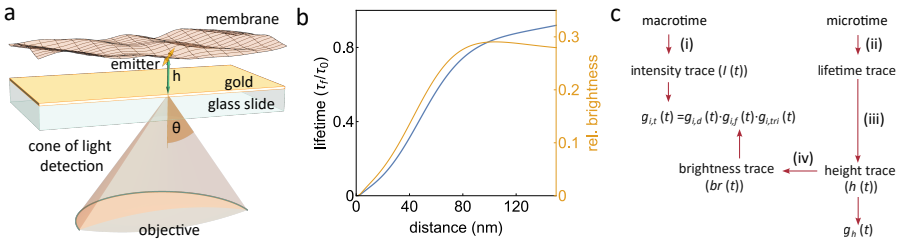

Fig. 1 Principle of MIET-FCS for measuring membrane dynamics. (a) A fluctuating membrane situated above a gold film is schematically depicted. The yellow arrow symbolizes an emitter dipole on the membrane, while the green arrow represents the height of this emitter from the substrate. (b) Calculated relative fluorescence lifetime τ_f/τ_0 (upper panel) and relative brightness (lower panel) of an emitter as a function of its distance h from the surface of a 10 nm gold film. These calculations consider an emitter with a maximum emission wavelength of 680 nm, a fluorescence quantum yield of 0.8, and a random orientation. (c) MIET-FCS analysis flow chart.

photons is timed with a multichannel picosecond event timer, so that fluorescence lifetime measurements can be done via time-correlated single-photon counting (TCSPC).

MIET relies on the electrodynamic coupling of the near-field of an excited fluorophore to surface plasmons in the metal film. In this coupling, the thin metal film (e.g., Au) functions as an acceptor for the excited state energy of an excited fluorophore, similar to fluorescent acceptor in Förster resonance energy transfer (FRET). The coupling is highly distance-dependent, leading to a distinct modulation of the fluorescence lifetime and brightness of the fluorophore as a function of its distance from the metal film.

This fluorophore-metal interaction can be modeled in a semi-classical approach based on Maxwell's equations. For this purpose, one considers the fluorescent molecule as an ideal electric dipole emitter and calculates its electromagnetic field in the presence of the MIET (GIET) substrate, as detailed in Refs. [37, 38]. This allows for the calculation of the total dipole emission rate (inverse radiative decay rate of the excited fluorophore) as a function of dipole position, orientation (expressed by the angle β between its dipole axis and the vertical direction) and geometry and electrodynamic properties (complex-valued refractive indices) of the substrate. Together with the knowledge of the fluorescence quantum yield ϕ (the ratio of radiative to total transition rate), one then obtains values of the observable fluorescence lifetime $\tau_f(h,\beta)$ and brightness $b(h,\beta)$ of a fluorophore as a function of its distance h and orientation angle β as

$$\frac{\tau_f(h,\beta)}{\tau_0} = \frac{S_0}{\phi S(h,\beta) + (1-\phi)S_0} \tag{1}$$

$$b(h,\beta) \propto \int_0^{\pi/2} d\beta \sin\beta \frac{N(h,\beta)}{S(h,\beta)} C(h,\beta) \tag{2}$$

In Eq. 1, $S(h,\beta)$ represents the total emission power of the emitter, where S_0 stands for the emission power of an electric dipole emitter with unity quantum yield in a homogeneous unbounded dielectric medium with a refractive index n, where the emitter has fluorescence lifetime τ_0 (free-space fluorescence lifetime). Moving to Eq 2, $N(h,\beta)$ is the total far-field emission radiated into the lower half space (glass coverslip), while $C(h,\beta)$ signifies the relative proportion of emission collected by the objective lens. The angular dependence of $S(h,\beta)$ can be decomposed as $S(h,\beta) = S_\perp(h)\cos^2\beta + S_\parallel(h)\sin^2\beta$, where $S_\perp(h)$ and $S_\parallel(h)$ are the radiative emission rates of emitters oriented perpendicular and parallel to the substrate, respectively. This decomposition extends similarly to $N(h,\beta)$ and $C(h,\beta)$. A detailed mathematical explanation is given in Ref. [39]. It is crucial to note that the functions $S_\perp(h)$ and $S_\parallel(h)$ are solely dependent on h.

Figure 1b presents calculations of the relative fluorescence lifetime $\tau_f(h)/\tau_0$ and relative brightness $b(h)$ for a rapidly rotating dye (averaging over all orientation angles) with a quantum yield of $\phi = 0.8$, emitting at $\lambda_{\mathrm{em}} = 680$ nm, as a function of height h over a gold-coated coverslip. The fluorescence lifetime exhibits a monotonic increase within a distance of up to approximately 200 nm, while the relative brightness peaks already at around 90 nm distance from the substrate surface.

The distance-dependent detectable fluorescence brightness is particularly important for the current study, as it allows in combination with FCS to measure minute vertical membrane fluctuations near a MIET substrate. In the absence of a MIET substrate (conventional FCS measurement), FCS would predominantly capture intensity fluctuations resulting from the lateral diffusion of labeled lipids through the confocal volume (Figure 1c). However, in the presence of a MIET substrate, these intensity fluctuations are also induced by vertical position fluctuations of the membrane (Figure 1b). Thus, measured fluorescence intensity fluctuations arise from two contributions: lateral diffusion and height fluctuation near the MIET substrate.

Measured fluorescence intensity fluctuations can be analyzed by calculating an intensity autocorrelation function $g_{i,t}(t)$ (iACF). The value of the iACF for a lag time t is defined as the time average of the product of intensity deviations from the mean value at time, t' $\delta I(t') = I(t') - \langle I \rangle$, and at time $t'+t$, $\delta I(t'+t) = I(t'+t) - \langle I \rangle$, i.e. $g_i(t) = \langle \delta I(t')\delta I(t'+t) \rangle$, where the angular brackets denote averaging over time t'. As mentioned above, in the presence of a MIET substrate, the total iACF $g_{i,t}(t)$ can be divided into a part $g_{i,d}(t)$ related to the lateral diffusion of single lipids, a part $g_{i,f}(t)$ related to vertical undulations of the membrane, and a part $g_{i,tri}(t)$ related to the triple state relaxation of the fluorophore:

$$g_{i,t}(t) = g_{i,d}(t) \cdot g_{i,f}(t) \cdot g_{i,tri}(t) \tag{3}$$

The triplet state relaxation rate is typically very fast, occurring within the range of nanoseconds to microseconds, which is much faster than the rate of membrane dynamics. Therefore, the presence of the triplet state should

not affect the dynamics fitting. However, the challenge remains in how best to distinguish between the contributions from diffusion and fluctuation when measuring only the total intensity autocorrelation function iACF $g_{i,t}$. One approach is to use a high labeling concentration when labeling the membrane lipids, which leads to a suppression of the diffusion-related but in the iACF, because the amplitude of this diffusion-related part is inversely proportional to dye concentration (or average number N of molecules in the focal volume) [36]. However, in this approach, one cannot gain any information about the lateral diffusion of lipids within a membrane. Here, we introduce an alternative strategy that concurrently extracts information on fluorescence lifetime, height, and brightness to study both lipid diffusion and membrane undulations. This is achieved by so-called time-tagged time-resolved (TTTR) single-photon counting. For each detected photon, TTTR provides two timestamps: the macrotime that counts the number of laser pulses between the start of the measurement and the photon detection, and the microtime that is the delay time between the last laser pulse and the photon detection. The macrotime is utilized for computing intensity traces and the iACF $g_{i,t}$, while the microtime is used to calculate the fluorescence lifetime via TCSPC.

In our MIET-FCS analysis (Figure 1c), we start with computing an intensity trace $I(t)$ over time bins with width Δ t = 100 µs or 1ms, which is then used to calculate the iACF $g_{i,t}(t)$ (after photobleaching correction, see Supplementary Figure 1 and Supplementary Note 1). Subsequently, we determine the fluorescence lifetime within each time bin by computing the square root of the variance of the microtimes recorded during each time bin. An ideal fast lifetime estimation should have less than 10 % uncertainty, which requires approximately 100 photons [40, 41]. This determines the minimum width of the time binning: one needs approximately 100 photons per time bin for a reasonable lifetime estimate. Taking into account that the maximum photon detection rate that a single photon detector can handle is typically around 4,000 kcps (kilo counts per second), one obtains a minimal possible time bin width of 25 µs. However, the photon detection rate varies as a function of fluorophore brightness and concentration, which results in a varying temporal resolution for different samples (see Supplementary Note 2 and Supplementary Figure 2).

In a next step, each fluorescence lifetime per time bin is converted into a height value using the lifetime-versus-height calibration curve (Figure 1), resulting in a continuous trace of height values $h(t)$. Furthermore, relying on the brightness-height calibration curve, a relative brightness trace ($br(t)$) is obtained, facilitating the direct computation of the MIET-induced height-related correlation function ($g_{i,f}(t) = \langle br(t')br(t'+t)\rangle_{t'} / \langle br(t)\rangle^2$). For $g_{i,d}(t)$, the diffusion can be described with a 2D diffusion model, $g_{i,d} = 1/(N(1 + t/t_D))$, where N is the total molecules in the confocal volume and τ_D is the diffusion time of lipids through the confocal volume Therefore, from Eq. 3, combining all the contributions, the iACF $g_{i,t}(t)$ can be fitted with following

model:

$$g_{i,t}(t) = \left[1 + \frac{F\exp(-t/\tau_T)}{1-F}\right] \frac{g_{i,f}(t)}{N(1+t/\tau_D)} \tag{4}$$

where F and τ_T are the triplet state amplitude and time that take into account the triplet state pumping and decay of the used fluorophores. Finally, the diffusion coefficient D is determined from $D = w^2/(4\tau_D)$, where w is the beam waist of the laser excitation focus in the plane of the membrane.

The height trace $h(t)$ provides information about the vertical undulations of a membrane. It can be decomposed into a mean value h_0 plus a deviation from this mean value $\delta h(t)$, i.e. $h(t) = h_0 + \delta h(t)$. The temporal dynamics of these membrane undulations can be characterized by the height autocorrelation function $g_h(t) = \langle \delta h(t')\delta h(t'+t)\rangle_{t'}$ (hACF).

Next, we can utilize the hACF $g_h(t)$ and the diffusion-related iACF $g_{\mathrm{dif}}(t)$ to analyze the 3D dynamics of the membrane. The amplitude of the hACF $g_h(t)$ determines the mean displacement amplitude ($\psi = \sqrt{<\delta h^2>}$), and the decay time of the hACF, determined by the point where this function has decreased to half its maximum value, yields a relaxation time τ^*.

3D dynamics of GUV membranes

We validated MIET-FCS by measuring membrane undulations and lipid diffusion in the proximal membrane of deflated giant unilamellar vesicles (GUVs), and then comparing our measurements with well-established theoretical predictions [42–45], previous experimental results [11, 36, 42–44], and a comparison to a planar membrane without bending undulations. GUVs were prepared from 1-stearoyl-2-oleoyl-sn-glycero-3-phosphocholine (SOPC) lipids and fluorescently labeled 1,2-Dipalmitoyl-sn-glycero-3-phosphoethanolamine (DPPE-Atto655) in a labeling ratio of 0.05 mol% by electroformation in a sucrose solution with an osmotic pressure of 230 mOsm/L. For the fluorescence measurements, see Figure 2a, GUVs were immersed in a hypertonic solution of 400 mOsm/L and added above a MIET substrate that was passivated with bovine serum albumin (BSA). The MIET substrate comprised of a 10 nm thick silica layer and a 10 nm gold film on a glass coverslip. The elevated osmolarity outside the GUVs led to their deflation and reduction of membrane tension, inducing membrane undulations even close to the substrate surface [11, 23]. FCS measurements were performed while focusing the laser focus at the bottom of the chamber within the contact area of the GUV's bottom membrane.

GUV deflation was evidenced by the non-circular geometry of the contact area between the GUV and the MIET substrate (Figure 2a). Figure 2b-i displays a measured intensity trace $I(t)$ with a time bin width of 100 µs, where the mean number of photons per time bin was ~ 210. The height trace $h(t)$, Figure 2b-ii, and brightness trace $b(t)$, Figure 2b-iii, were calculated from the

lifetime values of each time bin and converted into height and intensity values using the lifetime-versus-height calibration and height-versus-brightness calibration curves (Figure 1). Figure 2 shows the various obtained ACFs:

- the total iACF $g_i(t)$ (green dots), calculated from $I(t)$, revealing two decay components with distinct decay times
- the diffusion-related iACF g_{dif} (yellow line), calculated from $b(t)$
- the diffusion-related iACF g_{dif} (blue line), calculated via eq 3

As can be seen, we successfully separated iACF into contributions from lateral lipid diffusion and from vertical undulations of the membrane. Moreover, we determined the translational diffusion coefficient of the membrane lipids as D = 6.75 $\mu m^2/s$ by fitting the iACF $g_i(t)$ with Eq 5 (green line). This value of diffusion coefficient aligns well with values measured for deflated GUVs on a pure glass substrate (Supplementary Figure 3), where vertical membrane undulations to not contribute to fluorescence intensity fluctuations.

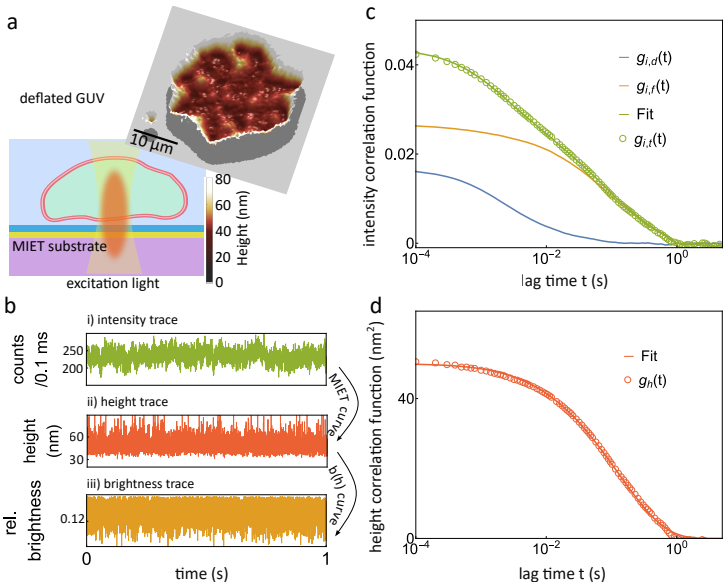

Fig. 2 Validation of MIET-FCS on model GUV membrane. (a) Schematic of a MIET-FCS experiment on a GUV above a MIET substrate. In the upper panel, exemplary 3D reconstructions (height image) of the proximal membrane of a deflated GUV on a MIET substrate are shown, with height encoded by color. (b) Calculated fluorescence intensity time trace (i), height trace (ii), and brightness trace (iii) for the proximal membrane of one deflated GUV. (c) Various fluorescence iACFs derived from measurements of the proximal membrane of surface-immobilized GUVs on a MIET substrate. The green solid line represents a fit with Eq. 4. (d) Calculated hACF (dotted lines) for the same deflated GUV. Fit values obtained from fitting the hACF with eq 5 (solid line) are also shown.

We subsequently derived a hACF to assess the vertical membrane undulations (Figure 2d). It is evident that the membrane height fluctuations of the

deflated GUVs exhibit a larger amplitude, characterized by a root-mean-square height fluctuation of $\psi = 6.6 \pm 3.2$ nm and a relaxation time of $\tau^* = 59 \pm 55$ ms (mean $\pm$ SD, $n = 65$). This observation concurs with our prior measurements utilizing a high label-concentration method and MIET-FCS, and aligns well with values obtained by other techniques [42].

The measured hACF $g_h(t)$ can be effectively modeled using a theoretical framework outlined in Refs. [42–45]). The model parameters are the membrane bending rigidity κ, the membrane tension σ, the effective viscosity η, and an effective interaction potential γ characterizing the interplay between the fluctuating membrane and the substrate surface. The hACF is modeled by the following equation:

$$\langle \delta h(t')\delta h(t'+t)\rangle_{t'} = \frac{k_B T}{2\pi}\int_{q_{\min}}^{q_{\max}} dq \frac{q}{\kappa q^4 + \sigma q^2 + \gamma} \exp\left[-\Gamma(q)t - \frac{1}{4}w^2 q^2\right] \tag{5}$$

where w denotes the diameter of the confocal detection area. The function $\Gamma(q)$ is defined by

$$\Gamma(q) = \frac{\kappa q^4 + \sigma q^2 + \gamma}{2\eta q} \frac{\sinh^2(qh_0) - (qh_0)^2}{\sinh^2(qh_0) + \sinh(2qh_0)/2 + qh_0(1 - qh_0)} \tag{6}$$

The integration boundaries of the integral in eq. (5) are $q_{\min} = (\gamma/\kappa)^{1/4}$ and $q_{\max} = 1/h_0$ [45].

When applying this model for describing the hACF of SOPC membranes, we fixed the value of the bending modulus to $\kappa = 20\, k_B T$ as reported in the literature [11, 46]. The effective viscosity $\eta = 1.2$ mPas was computed as the arithmetic mean of the viscosity of the buffer solutions inside and outside the GUV. The diameter of the confocal detection area in our measurement was determined as $w = 280$ nm by measuring the FCS of a sample with a known diffusion coefficient. We performed 65 measurements and fits of hACFs, a representative curve (same data point for Figure 2c) and fit is shown in Figure 2d. From these fits, we derived a surface tension value of $\sigma = 13 \pm 12$ µJm^{-2} (mean $\pm$ SD, n = 65) and an interaction potential strength value of $\gamma = 8 \pm 6$ MJm^{-4} (mean $\pm$ SD, n = 65), in excellent agreement with published results for similar GUVs [36, 42–44].

As a control measurement, we conducted MIET-FCS measurements on a supported lipid bilayer (SLB) on a MIET substrate with a 40 nm silica spacer (Figure 3a). We compared the parameter values obtained from the SLB measurments with those obtained from the measurements on deflated GUVs (Figure 3b). An SLB is a planar membrane on a substrate with only a thin hydration layer of only $1 \sim 2$ nm between the substrate and the membrane (Figure 3a). Consequently, an SLB can be considered as a membrane without vertical undulations. As anticipated, the brightness-related iACF is nearly flat, indicating that all intensity fluctuations arise from the lateral diffusion of lipid

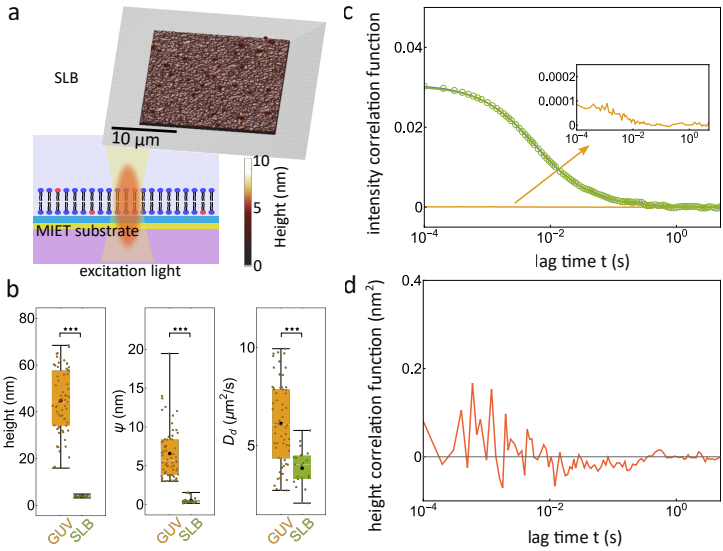

Fig. 3 MIET-FCS on model SLB. (a) Schematic of a MIET-FCS experiment on a SLB deposited on a MIET substrate. In the upper panel, exemplary 3D height profiles of the SLB on the MIET substrate. Height values are encoded by color. (b) Box plots for mean height value h_0, height correlation amplitude ψ, and diffusion coefficient D. Box plots show the 25th–75th quantiles (box), median (white line), mean (black dot), and whiskers (minima to maxima). We performed $n = 22$ independent measurements over 2 independent experiments for SLBs, and $n = 65$ independent measurements over 4 independent experiments for deflated GUVs. Significance levels P were evaluated by a Mann-Whitney U-test: $P < 0.001$ ($\star\star\star$), $P < 0.01$ ($\star\star$), $P < 0.05$ ($\star$). (c) Fluorescence iACFs derived from planar SLB supported on a MIET substrate. The green solid line is fitted with eq 4. Inset shows an enlarged plot of the height-fluctuation-related iACF. (d) Calculated hACF (dotted lines) for the same SLB.

molecules (Figure 3c). Similarly, the observed hACF amplitude for an SLB is negligible ($\psi = 0.54 \pm 0.41$ nm, mean ± SD, n = 22, Figure 3d).

The diffusion coefficients for deflated GUVs obtained with MIET-FCS and with conventional FCS (measuring on glass for deflated GUV, see Supplementary Figure 3) are very close to each other (MIET-FCS: 6.13 ± 2.03 µm²/s; conventional FCS: 6.5 ± 2.0 µm²/s). It should be noted that the diffusion coefficient $D = 3.85 \pm 0.95$ µm²/s ($n = 22$) of lipid diffusion in an SLB is considerably slower than that of lipids in a deflated GUV ($D = 6.13 \pm 2.03$ µm²/s, $n = 65$). This difference is due to the fact that lipid diffusion in the proximal leaflet of an SLB is impeded by stong interaction between lipids and the solid support, while for a deflated GUV, the interaction is less pronounced due to the larger distance of the membrane from the substrate.

The 3D membrane dynamics as measured with MIET-FCS, aligns well with existing theoretical models and provides reliable values for parameters such as diffusion coefficient, undulation amplitudes, membrane tension, and energy dissipation. Thus, MIET-FCS is an accurate and reliable technique, and we apply it next to studying more complex membranes of living cells.

3D dynamics of the cellular plasma membrane

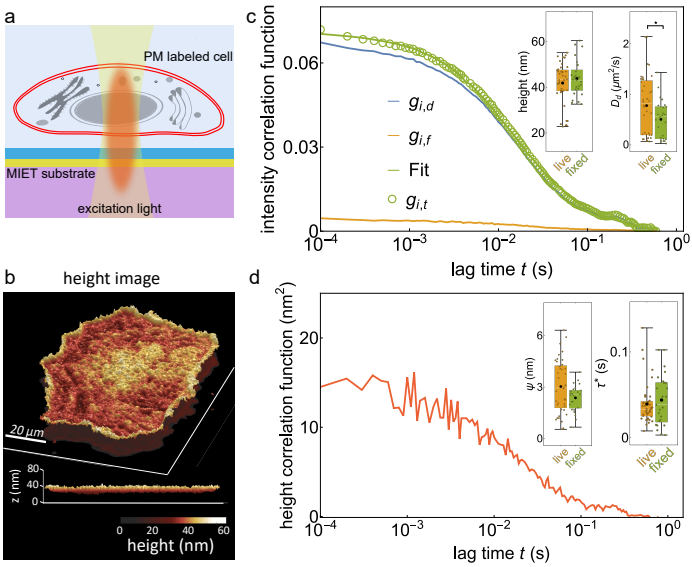

Fig. 4 MIET-FCS measurement on a cellular PM. (a) A schematic of the MIET-FCS experiment conducted on a PM-labeled cell on top of a MIET substrate. (b) Reconstructed 3D topography of the fluorescently labeled basal plasma membrane of a living Cos7 cell on a MIET substrate. The bottom panel offers an alternative viewing angle. Height is color-coded for clarity. (c,d) Same as Figure 2c,d, but for PM system. $n = 40$ independent measurements over 3 independent experiments for living cells, and $n = 25$ independent measurements over 2 independent experiments for fixed cells. Insets show box plots of mean height values h_0, diffusion coefficients D, fluctuation amplitudes ψ, and relaxation times $\tau*$ for living and fixed cells.

The plasma membrane (PM) is a very dynamic structure involved in various cellular functions, including cell motility, cell division, or vesicle trafficking. The PM undulations span a broad temporal range, with slow actin waves inducing large wavelength membrane oscillations at cell edges with time durations of seconds. These oscillations involve perpendicular membrane undulations ranging from 100 nm to 10 µm [47]. In the basal membrane, smaller amplitude undulations are observed, due to the presence of the extracellular matrix (ECM) between the PM and the substrate. While larger undulation amplitudes are linked to cell spreading and motility, even small undulations can influence the spatial organization of embedded molecules within the PM, contributing to the formation of nanodomains or invaginations [48].

We applied MIET-FCS to measure the 3D dynamics of the basal membrane COS7 cells cultured on a MIET substrate with a 10 nm silica spacer, where the PM was labeled with the commercial PM stain CellMask Deep Red. MIET-FCS measurements were performed on the basal membrane of both living and fixed cells (Figure 4a). Figure 4b displays reconstructed 3D height maps

of the basal membrane of COS7 cells. As can be seen, the distance between basal membrane and substrate varies between 35 to 55 nm. We randomly chose different points in different cells for point measurement of the temporal dynamics of PM undulations.

Figure 4c shows that average height values of the membrane appear unaffected by the biological activity of a cell, measuring 41.9 ± 9.2 nm (mean ± SD, $n = 40$) in living cells and 43.8 ± 7.9 nm (mean ± SD, $n = 25$) in fixed cells. Notably, faster lipid diffusion was observed in living cells, with a 1.5-fold increase compared to fixed cells. Specifically, diffusion coefficients were 0.50 ± 0.38 $\mu m^2/s$ for fixed cells and 0.77 ± 0.59 $\mu m^2/s$ for living cells. Unexpectedly, PM undulations were minimal in both living and fixed cells (Figure 4d). Living cells exhibited only ∼1.3 times larger undulation amplitudes (3.03 ± 1.54 nm) and ∼1.4 times slower fluctuation times (28 ± 23 ms) than fixed cells (2.37 ± 0.75 nm and 39 ± 24 ms, respectively). Considering that cross-linked proteins in fixed cells hinder active dynamics, our observations suggest that both the active (ATP-dependent) and passive (thermal fluctuations) processes contribute to the basal PM dynamics, in agreement with previous findings using alternative techniques [48]. The increase in fluctuation time after cell fixation implies a stiffening of the PM [49].

3D dynamics of endoplasmic reticulum

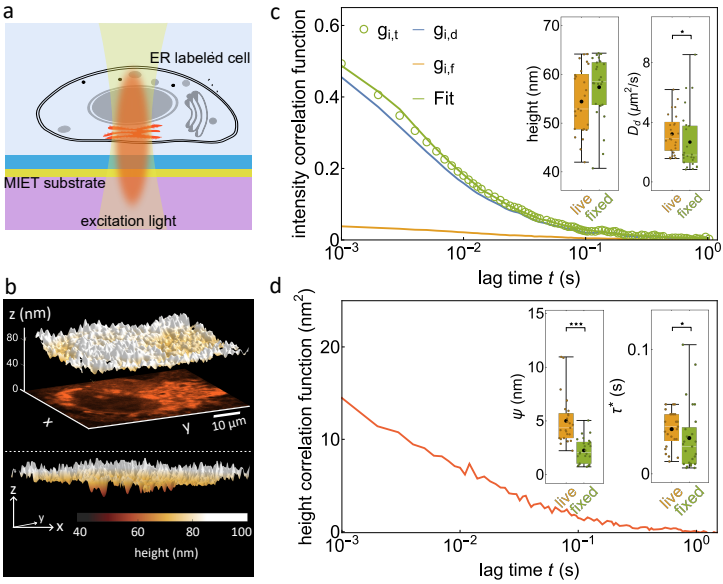

Fig. 5 MIET-FCS measurement on ER. (a,c,d) Same as Figure 3a,c,d, but for ER system. $n = 25$ independent measurements over 3 independent experiments for both living cells and fixed cells. (b) Exemplary three-dimensional reconstructions (height maps) of fluorescently labeled ER in a live COS7 cell on a MIET substrate. The xy-image shows the fluorescence intensity. Bottom panel shows the height image from a different viewing angle.

The endoplasmic reticulum (ER) is a sub-cellular organelle responsible for numerous essential cellular processes. Within living cells, the ER exhibits high dynamism, continuously undergoing shape remodeling. While the relationship between ER dynamics and function is not fully understood, recent findings associate abnormal ER dynamics with various diseases [50]. Previous reports have categorized ER dynamics in mammalian cells into three types: oscillations of established network elements, dynamics of particles within the ER lumen or membrane, and generation of new network elements [50]. Quantifying ER dynamics remains a formidable challenge due to the complex nature of its movement.

We employed MIET-FCS to measure the 3D dynamics of ER in COS7 cells on a MIET substrate with a 10 nm silica spacer (Figure 5a). For live-cell imaging, the ER was labeled with the commercial dye ER-Tracker Red. In Figure 5b, we present 3D reconstructed height maps of the labeled ER in a living cell. The distance between substrate and ER exhibits considerable variation, ranging from 50 nm to 120 nm. It is important to note that the signal observed from a confocal microscope represents a spatial average over the size of the excitation focus (approximately 300 nm) and over vertical regions of around 500 nm (Figure 5a). Therefore, the height images in Figure 5b do not depict a single ER bilayer, but rather an average value across the confocal volume. Notably, some locations in Figure 5b show very low height values (approximately 50 nm), which we attribute to contact sites between the ER and the PM [51].

While performing point measurements on the ER, it happens that certain parts of the ER are within confocal volume but beyond the working distance of MIET (approximately 200 nm from the surface). The signal from ER regions outside the MIET working distance can impact the measured results of ER within the MIET working range. To minimize the impact of out-of-MIET ER contributions, we excluded data for which the ER height was larger than 65 nm (see Supplementary Figure 4 and Supplementary Note 3).

As depicted in Figure 5c and d, we can distinguish between the lateral lipid diffusion and perpendicular membrane undulation components in ER dynamics. Comparative MIET-FCS experiments were conducted on living and fixed cells. Our findings do not reveal a significant difference in average membrane height h_0 in both cases, with measured values of 54.4 ± 6.7 nm for living cells and 57.4 ± 6.5 nm for fixed cells (mean ± SD, $n = 25$ for living cells and $n = 25$ for fixed cells).

However, significant differences are observed for other parameters. The fluctuation amplitude ψ exhibits a 50% decrease in fixed cells compared to living cells, measuring 5.0 ± 2.2 nm for living cells and 2.3 ± 1.2 nm for fixed cells. The diffusion coefficient in living cells decreased by approximately 17% from its value compared in fixed cells, measuring 3.2 ± 1.3 $\mu m^2/s$ for living cells and 2.7 ± 2.0 $\mu m^2/s$ for fixed cells. Finally, the correlation relaxation time τ^* showed a 20% decrease from 36 ± 14 ms in living cells to 28 ± 26 ms in fixed cells. The substantial reduction in the undulation amplitude ψ from

living to fixed cells can be attributed to the fact that the ER dynamics is predominantly determined by the active motion of the cytoskeleton network and motor proteins [52, 53].

3D dynamics of the nuclear envelope

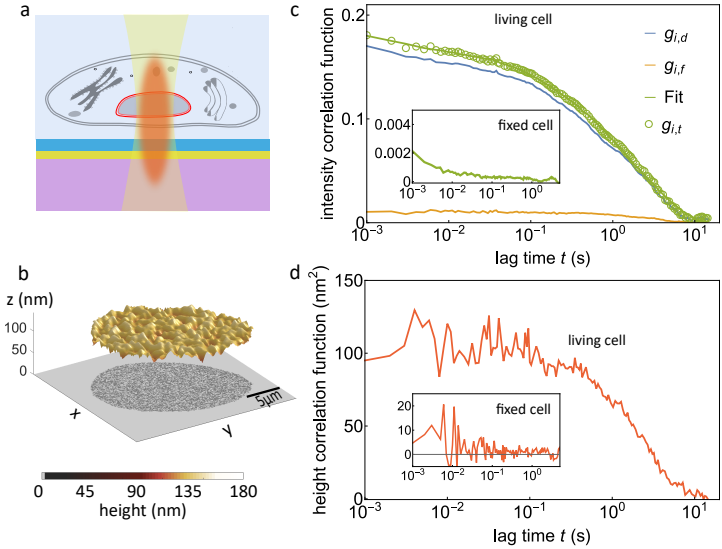

Fig. 6 MIET-FCS measurement of NE dynamics. (a, b) Same as Figure 2a, b, but for NE system. (c) iACFs obtained for living eGFP-nup153-modified COS7 cell. The green solid line represents a fit with eq 4. Inset shows measured g_i for a fixed cell. (d) Calculated hACF for a living and a fixed cell (inset).

The nuclear envelope (NE) is the physical boundary between the cytoplasm and the nucleoplasm between two highly active systems, the cellular cytoskeleton and the nuclear chromatin. We performed MIET-FCS measurements on live and fixed COS7 cells expressing eGFP fused to the nuclear pore protein Nup153, see Figure 6a and Supplementary Figure 5. Figure 6b shows the measured height profile of the proximal part of the nuclear envelope, showing an average height value of approximately 130 nm well within the working distance of MIET.

Figure 6c shows iACFs for NE Nup153 lateral diffusion and membrane undulations in living cells. The observed diffusion is ca. 100 times slower than values measured for lipid diffusion in deflated GUVs, with a diffusion coefficient of only 0.0059 ± 0.0040 µm^2/s ($n = 33$). The relaxation time of NE membrane undulations is also 60 times slower than that for deflated GUV, determined to be on the timescale of seconds (3.6 ± 1.6 s), in good agreement with previous measurements [54, 55]. The slower dynamics of the NE compared to other cellular membranes can be attributed to its double-bilayer structure, and to

strong links to the cytoskeleton on the cytoplasmic side and to the chromatin on the nucleoplasmic side.

As expected, no diffusion or undulations were observed in fixed cells (Figure 6c,d inset), where the amplitude of the measured total iACF is only 0.002 or 100 times smaller than its value measured in living cells. The small residual iACF amplitude may be due triplet-state dynamics of the eGFP labels. The hACF is too noisy to allow for determining reliable values of relaxation time and amplitude. We attribute the absence of sensible NE dynamics in fixed cells to fixation-induced cross-linking of cellular proteins.

Discussion

In this study, we introduced MIET-FCS for measuring the 3D dynamics of various membrane systems, both *in vitro* and *in vivo*. MIET-FCS combines the nanometer axial resolution of MIET with the 100 µs to 1 ms temporal resolution of the intensity and lifetime time traces, enabling the simultaneous tracking of in-membrane diffusion and transversal membrane undulations. MIET-FCS is straightforward to implement using standard confocal microscopy, and calibration curves are exactly calculated without the need of independent experimental calibration.

We demonstrated the versatility of MIET-FCS for a wide range of membrane biophysical studies, including measurements on GUV membranes, and cellular PM, ER, and NE. We showed how to extract multiple physical parameters such as diffusion coefficients, undulation amplitudes and relaxation times, as well as values for membrane tension and and membrane-substrate interaction strengths in GUV measurements. This capability is particularly valuable for uncovering membrane-substrate interactions and for investigating the correlation between membrane undulations and lipid diffusion. Beyond model membranes, we demonstrated the usefulness of MIET-FCS for membrane studies in living and fixed cells.

Methods

The research conducted in this study complies with all relevant ethical regulations.

MIET-FCS measurement

MIET-FCS measurements were conducted using a custom-built confocal microscopy setup. The excitation sources comprised a pulsed diode laser (λ_{exc} = 640nm, LDH-D-C 640, PicoQuant) for red dye and a white laser (xx) with Acousto-Optic Tunable Filters (AOTFnC-400.650-TN, Pegasus Optik Gmbh). The beam was collimated from an infinity-corrected 4x objective (UPISApo 4X, Olympus), then reflected by a dichroic mirror (Di01-R405/488/561/635, Semrock) towards a high numerical aperture objective (UApoN 100X, oil, 1.49 N.A., Olympus). Emission light was focused into a pinhole with a diameter of

100 μm and refocused onto two avalanche photodiodes (τ-SPAD, PicoQuant). A long-pass filter (BLP01-647R-25, or LF561/LP-D-000, or LF488/LP-C-000, Semrock) and two band-pass filters (Brightline HC692/40, or FF01-609/54-25, or FF01-525/45-25, Semrock) were positioned before the pinhole and the detector, respectively. Single-count data from the detector were processed using a multi-channel picosecond event timer (Hydraharp 400, PicoQuant). Imaging scanning was facilitated by a fast Galvo scanner (FLIMbee, Picoquant).

For live cell measurements, a microscopy-based incubator (ibidi Stage Top Incubation System-Blue Line, ibidi) maintained controlled conditions (temperature: 37 °C, CO_2 concentration: 5%, humidity: 40%). In a typical measurement, the sample was initially scanned at the MIET substrate surface to determine the contour of the GUVs or cells. Subsequently, an appropriate point position was selected for single-point acquisition, and data were recorded for at least 2 minutes for each data point. The sample within the working distance of MIET can be determined by its fluorescene curve (see Supplementary Figure 6).

Substrate preparation

We followed the procedures outlined in our previous publications [35, 38] to prepare the gold-modified substrate. A layer-by-layer deposition technique was used, where 2 nm of titanium, 10 nm of gold, 1 nm of titanium, and 10 nm of SiO_2 were successively electron-beam evaporated onto the surface of a glass coverslip. The electron-beam evaporation was carried out using a Univex 350 electron beam source (Leybold) under high-vacuum conditions (approximately 10^{-6} mbar). To ensure maximal homogeneity, the deposition was conducted at the slowest rate (1 $Å s^{-1}$). The spacer thickness was continuously monitored during the evaporation process using an oscillating quartz unit. This gold-covered substrate is referred to as the MIET substrate.

Prior to the MIET experiment, the MIET substrate underwent plasma cleaning for 60 seconds at the highest plasma intensity (Harrick Plasma). Subsequently, it was incubated in a 5 mg/mL^{-1} solution of bovine serum albumin (BSA, Sigma-Aldrich) for 15 minutes to prevent nonspecific interactions in GUV experiments.

Vesicles and SLB preparation

SLB was prepared through the fusion of small unilamellar vesicles (SUVs), which were generated using an extrusion method. A 100 μL mixture containing 10 mg/mL 1,2-Dioleoyl-sn-glycero-3-phosphocholine (DOPC) lipids and 0.05 mol% DPPE-atto655 lipids in chloroform was dried in a vacuum for 1 h at 30 °C. The resulting lipid film was then re-dispersed in 500 μL of PBS buffer (pH = 7.4) and shaken for 1 h at 37 °C. SUVs were obtained by extruding the solution through a polycarbonate filter (Whatman) with a 50 nm pore diameter for 15 cycles. The SLB was prepared by incubating the SUV solution on the MIET substrate for 1 h at room temperature, followed by washing with PBS buffer.

GUVs made of SOPC were fabricated using the electroformation method [38]. A 100 μL lipid mixture containing 10 mg/mL SOPC, 2 mol% 1,2-dioleoyl-sn-glycero-3-phosphoethanolamine-N-(methoxy(polyethylene glycol)-2000) (DOPE-PEG2000), and 0.05 mol% DPPE-atto655 was deposited on two steel electrodes and evaporated for 3 h under vacuum at 30 °C. The electrodes were sealed with a Teflon chamber and filled with 500 μL of sucrose solution (230 mM). The chamber was subjected to an alternating electric current at 15 Hz for 3 h with a peak-to-peak voltage of 1.6, followed by 8 Hz for 30 min. After electro-formation, the GUVs suspension was stored at −4°C and used within 3 days. The GUVs suspension was diluted 50 times in PBS buffer (400 $mOsml^{-1}$, 10mM Na_2HPO_4, 2mM KH_2PO_4, 3 mM KCl, and 180 mM NaCl, pH 7.4) for the observation of floppy GUVs. For all GUV experiments, the diluted GUVs solution with observation buffer was added to a chamber (Culture-Insert 4 Well, ibidi GmbH) on the MIET substrate. A glass slide covered the chamber, and the setup was left undisturbed for 10 min at room temperature for equilibration before the measurement.

Cell culture and mambrane labeling

COS7 monkey kidney cells were cultured at 37°C in 5% CO2 in T-75 culture flasks using Dulbecco's Modified Eagle's Medium (DMEM) - high glucose (Sigma, D6429-500L) supplemented with 10% fetal bovine serum (Sigma-Aldrich, F7524) and 1% penicillin/streptomycin (Sigma, P4333). Cells were seeded onto 35 mm glass-bottom dishes (Ibidi, 81158) coated or uncoated with gold at a concentration of 10^5 cells/dish and cultured for 24 hours. For fixed cells, cells were gently washed with PBS and then fixed in 4% paraformaldehyde/PBS solution for 20 minutes.

ER-Tracker Red (0.5 μM solution in DMEM) and CellMask Deep Red (500 ng/ml solution in DMEM) were used for specific labelling of the endoplasmic reticulum (ER) and plasma membrane (PM), respectively. In the case of the nucleus, the cells were transfected one day before use with the pEGFP(C3)-Nup153 plasmid encoding the fluorescent version of nucleoporin 153 [56] using Effectene Transfection Reagent (Qiagen, 301425). pEGFP(C3)-Nup153 was a gift from Birthe Fahrenkrog (Addgene plasmid # 64268; http://n2t.net/addgene:64268; RRID:Addgene_64268).

Statistics & Reproducibility

All values are expressed as the mean ± SD. All box plots show the 25th–75th quantiles (box), median (white line), mean (black dot), and whiskers (minima to maxima). Significance levels P were evaluated by a Mann-Whitney U-test: $P < 0.001$ ($\star\star\star$), $P < 0.01$ ($\star\star$), $P < 0.05$ ($\star$). No statistical method was used to predetermine sample size, and the sample size was chosen based on similar studies published before [11, 23]. All experiments were repeated at least twice with reproducible results.

Data Availability

Source data are provided with this paper. There are no restrictions on data availability. All data supporting the findings of this study are available within the main text, supplementary information, and 'Source data' Excel file.

Code Availability

All code used for generating Figures 1-6 are deposited on GitHub at https://gitlab.gwdg.de/tchen1/3dmembranedynamics.git. In particular, the depository contains:

- *Matlab* (v. 2022b, MathWorks® Inc.) code used for calculating the MIET and brightness calibration curves, intensity trace, height trace, intensity autocorrelation function, height autocorrelation function, as well as fitting the intensity autocorrelation function, height autocorrelation function;
- *Mathematica* (v. 13.2.1.0 Wolfram Research Inc.) notebook that generates the graphs of all figures;
- A Readme file to explain all analysis detials.

The 3D height profiles were calculated using a freely available MATLAB-based MIET-GUI software [57].

References

[1] Adhyapak, P., Kapoor, S.: Membrane dynamics in health and disease: impact on cellular signalling. The Journal of Membrane Biology **252**, 213–226 (2019)

[2] Julian, L., Olson, M.F.: Apoptotic membrane dynamics in health and disease. Cell Health and Cytoskeleton, 133–142 (2015)

[3] de Armas-Rillo, L., Valera, M.-S., Marrero-Hernández, S., Valenzuela-Fernández, A.: Membrane dynamics associated with viral infection. Reviews in medical virology **26**(3), 146–160 (2016)

[4] Linh, N.H., Man, V.H., Li, M.S., Wang, J., Derreumaux, P., Mai, T.L., Nguyen, P.H.: Molecular dynamics simulation of cancer cell membrane perforated by shockwave induced bubble collapse. The Journal of Chemical Physics **157**(22) (2022)

[5] Klauda, J.B., Roberts, M.F., Redfield, A.G., Brooks, B.R., Pastor, R.W.: Rotation of lipids in membranes: molecular dynamics simulation, 31p spin-lattice relaxation, and rigid-body dynamics. Biophysical journal **94**(8), 3074–3083 (2008)

[6] Javanainen, M., Ollila, O.S., Martinez-Seara, H.: Rotational diffusion of membrane proteins in crowded membranes. The Journal of Physical

Chemistry B **124**(15), 2994–3001 (2020)

[7] Miettinen, M.S., Lipowsky, R.: Bilayer membranes with frequent flip-flops have tensionless leaflets. Nano letters **19**(8), 5011–5016 (2019)

[8] Sanyal, S., Menon, A.K.: Flipping lipids: why an'what's the reason for? ACS chemical biology **4**(11), 895–909 (2009)

[9] Ramadurai, S., Holt, A., Krasnikov, V., Van Den Bogaart, G., Killian, J.A., Poolman, B.: Lateral diffusion of membrane proteins. Journal of the American Chemical Society **131**(35), 12650–12656 (2009)

[10] Almeida, P.F., Vaz, W.L.: Lateral diffusion in membranes. Handbook of biological physics **1**(C), 305–357 (1995)

[11] Monzel, C., Schmidt, D., Kleusch, C., Kirchenbüchler, D., Seifert, U., Smith, A., Sengupta, K., Merkel, R.: Measuring fast stochastic displacements of bio-membranes with dynamic optical displacement spectroscopy. Nature Communications **6**(1), 1–8 (2015)

[12] Turlier, H., Betz, T.: Unveiling the active nature of living-membrane fluctuations and mechanics. Annual Review of Condensed Matter Physics **10**, 213–232 (2019)

[13] McNiven, M.A., Ridley, A.J.: Focus on membrane dynamics. Trends in Cell Biology **16**(10), 485–486 (2006)

[14] Janmey, P., Kinnunen, P.K.: Biophysical properties of lipids and dynamic membranes. Trends in cell biology **16**(10), 538–546 (2006)

[15] Tomaiuolo, G.: Biomechanical properties of red blood cells in health and disease towards microfluidics. Biomicrofluidics **8**(5) (2014)

[16] Turlier, H., Fedosov, D.A., Audoly, B., Auth, T., Gov, N.S., Sykes, C., Joanny, J.-F., Gompper, G., Betz, T.: Equilibrium physics breakdown reveals the active nature of red blood cell flickering. Nature physics **12**(5), 513–519 (2016)

[17] Dulińska, I., Targosz, M., Strojny, W., Lekka, M., Czuba, P., Balwierz, W., Szymoński, M.: Stiffness of normal and pathological erythrocytes studied by means of atomic force microscopy. Journal of biochemical and biophysical methods **66**(1-3), 1–11 (2006)

[18] Kariuki, S.N., Marin-Menendez, A., Introini, V., Ravenhill, B.J., Lin, Y.-C., Macharia, A., Makale, J., Tendwa, M., Nyamu, W., Kotar, J., *et al.*: Red blood cell tension protects against severe malaria in the dantu blood group. Nature **585**(7826), 579–583 (2020)

[19] Ghanbarzadeh Nodehi, S., Shivashankar, G., Prost, J., Mohammad-Rafiee, F.: The characteristics of nuclear membrane fluctuations in stem cells. Journal of the Royal Society Interface **18**(176), 20201010 (2021)

[20] Goehring, N.W., Chowdhury, D., Hyman, A.A., Grill, S.W.: Frap analysis of membrane-associated proteins: lateral diffusion and membrane-cytoplasmic exchange. Biophysical Journal **99**(8), 2443–2452 (2010)

[21] Macháň, R., Hof, M.: Lipid diffusion in planar membranes investigated by fluorescence correlation spectroscopy. Biochimica et Biophysica Acta (BBA)-Biomembranes **1798**(7), 1377–1391 (2010)

[22] Weigel, A.V., Simon, B., Tamkun, M.M., Krapf, D.: Ergodic and non-ergodic processes coexist in the plasma membrane as observed by single-molecule tracking. Proceedings of the National Academy of Sciences **108**(16), 6438–6443 (2011)

[23] Monzel, C., Sengupta, K.: Measuring shape fluctuations in biological membranes. Journal of Physics D: Applied Physics **49**(24), 243002 (2016)

[24] Kaizuka, Y., Groves, J.T.: Hydrodynamic damping of membrane thermal fluctuations near surfaces imaged by fluorescence interference microscopy. Physical Review Letters **96**(11), 118101 (2006)

[25] Kaizuka, Y., Groves, J.T.: Structure and dynamics of supported intermembrane junctions. Biophysical Journal **86**(2), 905–912 (2004)

[26] Faris, M.E.A., Lacoste, D., Pécréaux, J., Joanny, J.-F., Prost, J., Bassereau, P.: Membrane tension lowering induced by protein activity. Physical Review Letters **102**(3), 038102 (2009)

[27] Brochard, F., Lennon, J.: Frequency spectrum of the flicker phenomenon in erythrocytes. Journal de Physique **36**(11), 1035–1047 (1975)

[28] Park, Y., Best, C.A., Auth, T., Gov, N.S., Safran, S.A., Popescu, G., Suresh, S., Feld, M.S.: Metabolic remodeling of the human red blood cell membrane. Proceedings of the National Academy of Sciences **107**(4), 1289–1294 (2010)

[29] Singh, V.R., Yang, Y.A., Yu, H., Kamm, R.D., Yaqoob, Z., So, P.T.: Studying nucleic envelope and plasma membrane mechanics of eukaryotic cells using confocal reflectance interferometric microscopy. Nature communications **10**(1), 3652 (2019)

[30] Sengupta, K., Limozin, L.: Adhesion of soft membranes controlled by tension and interfacial polymers. Physical Review Letters **104**(8), 088101 (2010)

[31] Smith, A.-S., Sengupta, K., Goennenwein, S., Seifert, U., Sackmann, E.: Force-induced growth of adhesion domains is controlled by receptor mobility. Proceedings of the National Academy of Sciences **105**(19), 6906–6911 (2008)

[32] Fenz, S.F., Bihr, T., Schmidt, D., Merkel, R., Seifert, U., Sengupta, K., Smith, A.-S.: Membrane fluctuations mediate lateral interaction between cadherin bonds. Nature Physics **13**(9), 906–913 (2017)

[33] Betz, T., Lenz, M., Joanny, J.-F., Sykes, C.: Atp-dependent mechanics of red blood cells. Proceedings of the National Academy of Sciences **106**(36), 15320–15325 (2009)

[34] Betz, T., Sykes, C.: Time resolved membrane fluctuation spectroscopy. Soft Matter **8**(19), 5317–5326 (2012)

[35] Chizhik, A.I., Rother, J., Gregor, I., Janshoff, A., Enderlein, J.: Metal-induced energy transfer for live cell nanoscopy. Nature Photonics **8**(2), 124–127 (2014)

[36] Chen, T., Karedla, N., Enderlein, J.: Measuring sub-nanometer fluctuations at microsecond temporal resolution with metal-and graphene-induced energy transfer spectroscopy. Nature communications **15**, 1789 (2024)

[37] Karedla, N., Chizhik, A.I., Gregor, I., Chizhik, A.M., Schulz, O., Enderlein, J.: Single-molecule metal-induced energy transfer (smmiet): Resolving nanometer distances at the single-molecule level. ChemPhysChem **15**(4), 705–711 (2014)

[38] Ghosh, A., Sharma, A., Chizhik, A.I., Isbaner, S., Ruhlandt, D., Tsukanov, R., Gregor, I., Karedla, N., Enderlein, J.: Graphene-based metal-induced energy transfer for sub-nanometre optical localization. Nature Photonics **13**(12), 860–865 (2019)

[39] Karedla, N., Chizhik, A.M., Stein, S.C., Ruhlandt, D., Gregor, I., Chizhik, A.I., Enderlein, J.: Three-dimensional single-molecule localization with nanometer accuracy using metal-induced energy transfer (miet) imaging. The Journal of Chemical Physics **148**(20), 204201 (2018)

[40] Liu, X., Lin, D., Becker, W., Niu, J., Yu, B., Liu, L., Qu, J.: Fast fluorescence lifetime imaging techniques: A review on challenge and development. Journal of Innovative Optical Health Sciences **12**(05), 1930003 (2019)

[41] Nasser, M., Meller, A.: Lifetime-based analysis of binary fluorophores mixtures in the low photon count limit. Iscience **25**(1) (2022)

[42] Rädler, J.O., Feder, T.J., Strey, H.H., Sackmann, E.: Fluctuation analysis of tension-controlled undulation forces between giant vesicles and solid substrates. Physical Review E **51**(5), 4526 (1995)

[43] Schmidt, D., Monzel, C., Bihr, T., Merkel, R., Seifert, U., Sengupta, K., Smith, A.-S.: Signature of a nonharmonic potential as revealed from a consistent shape and fluctuation analysis of an adherent membrane. Physical Review X **4**(2), 021023 (2014)

[44] Monzel, C., Schmidt, D., Seifert, U., Smith, A.-S., Merkel, R., Sengupta, K.: Nanometric thermal fluctuations of weakly confined biomembranes measured with microsecond time-resolution. Soft Matter **12**(21), 4755–4768 (2016)

[45] Gov, N., Zilman, A., Safran, S.: Hydrodynamics of confined membranes. Physical Review E **70**(1), 011104 (2004)

[46] Monzel, C., Fenz, S.F., Giesen, M., Merkel, R., Sengupta, K.: Mapping fluctuations in biomembranes adhered to micropatterns. Soft Matter **8**(22), 6128–6138 (2012)

[47] Giannone, G., Dubin-Thaler, B.J., Döbereiner, H.-G., Kieffer, N., Bresnick, A.R., Sheetz, M.P.: Periodic lamellipodial contractions correlate with rearward actin waves. Cell **116**(3), 431–443 (2004)

[48] Biswas, A., Alex, A., Sinha, B.: Mapping cell membrane fluctuations reveals their active regulation and transient heterogeneities. Biophysical Journal **113**(8), 1768–1781 (2017)

[49] Seifert, J., Rheinlaender, J., Novak, P., Korchev, Y.E., Schäffer, T.E.: Comparison of atomic force microscopy and scanning ion conductance microscopy for live cell imaging. Langmuir **31**(24), 6807–6813 (2015)

[50] Perkins, H.T., Allan, V.: Intertwined and finely balanced: endoplasmic reticulum morphology, dynamics, function, and diseases. Cells **10**(9), 2341 (2021)

[51] Fernández-Busnadiego, R., Saheki, Y., De Camilli, P.: Three-dimensional architecture of extended synaptotagmin-mediated endoplasmic reticulum–plasma membrane contact sites. Proceedings of the National Academy of Sciences **112**(16), 2004–2013 (2015)

[52] Hama, Y., Morishita, H., Mizushima, N.: Regulation of er-derived membrane dynamics by the deda domain-containing proteins vmp1 and tmem41b. EMBO reports **23**(2), 53894 (2022)

[53] Tikhomirova, M.S., Kadosh, A., Saukko-Paavola, A.J., Shemesh, T.,

Klemm, R.W.: A role for endoplasmic reticulum dynamics in the cellular distribution of microtubules. Proceedings of the National Academy of Sciences **119**(15), 2104309119 (2022)

[54] Introini, V., Kidiyoor, G.R., Porcella, G., Cicuta, P., Cosentino Lagomarsino, M.: Centripetal nuclear shape fluctuations associate with chromatin condensation in early prophase. Communications Biology **6**(1), 715 (2023)

[55] Chu, F.-Y., Haley, S.C., Zidovska, A.: On the origin of shape fluctuations of the cell nucleus. Proceedings of the National Academy of Sciences **114**(39), 10338–10343 (2017)

[56] Duheron, V., Chatel, G., Sauder, U., Oliveri, V., Fahrenkrog, B.: Structural characterization of altered nucleoporin nup153 expression in human cells by thin-section electron microscopy. Nucleus **5**(6), 601–612 (2014)

[57] Ghosh, A., Chizhik, A.I., Karedla, N., Enderlein, J.: Graphene-and metal-induced energy transfer for single-molecule imaging and live-cell nanoscopy with (sub)-nanometer axial resolution. Nature Protocols **16**(7), 3695–3715 (2021)

Acknowledgments

T.C. and J.E. acknowledge financial support by the European Research Council (ERC) for financial support via project “smMIET” (grant agreement no. 884488) under the European Union’s Horizon 2020 research and innovation program. J.E. acknowledges financial support by the DFG through Germany’s Excellence Strategy EXC 2067/1-390729940. J.I.G. acknowledges financial support from the European Union’s Horizon 2021 research and innovation program under the Marie Skłodowska-Curie Grant Agreement no. 101062508 (project name: SOADOPP). We thank Anna Chizhik, Ingo Gregor, and Alexey Chizhik for their help and support.

Author Contributions Statement

J.E. and T.C. conceived the project. T.C. prepared all samples of GUVs and SLBs. J.I.G. prepared most of the samples of cells and all genetically modified cells. T.C. and J.I.G. performed all the measurements. T.C. analyzed all the data and made all figures both in the main text and supplementary information. D.W prepared some cell samples for PM measurement. N.K. wrote part of MATLAB code to analyze the data. T.C. and J.I.G. helped with preparing the manuscript, which was written by J.E.

Competing Interests Statement

The authors declare no conflict of interest.